Ondra, V., Dibble, R., & Titurus, B. (2018). Towards an application of an active tendon in rotorcraft: A numerical and experimental study of coupled bending-torsion vibration of a beam-tendon system. In *28th International Conference on Noise and Vibration engineering (ISMA 2018)* (pp. 3645-3659). K U Leuven.

Peer reviewed version

Towards an application of an active tendon in rotorcraft: A numerical and experimental study of coupled bending-torsion vibration of a beam-tendon system

V. Ondra[1], **R. Dibble** [1], **B. Titurus**[1]
[1] University of Bristol, Department of Engineering,
Queen's Building, University Walk, Bristol, BS8 1TR, United Kingdom
e-mail: **vaclav.ondra@bristol.ac.uk**

Abstract
This paper presents a numerical and experimental study of coupled bending-torsion vibration of a beam loaded by a tendon-induced axial force. The rotating beam-tendon system is described using a set of partial differential equations and free vibration analysis is performed. The model is validated against a bench-top experiment which features a reinforced open-section cantilever beam subjected to tendon loading. A satisfactory agreement between the numerical and experimental results is obtained and it is shown that the tendon not only reduces the natural frequencies of the beam, but also introduces frequency loci veering. The validated model is then used to perform a case study on the Bo105 helicopter to present some benefits of incorporating a tendon in a rotorcraft blade, making a first step towards an active tendon concept. This concept should eventually allow rotorcraft to operate with a variable rotor speed, thereby increasing their performance and efficiency.

1 Introduction

In recent decades there has been a growing interest in many fields of technology, including civil, mechanical and aerospace engineering, in active and adaptive control of structures [1]. A far-reaching motivation of this study is to develop a new concept for rotorcraft blade control, whereby an active tensile member (hereafter referred to as a tendon) would be used as a means of adaptively manipulating a rotor's dynamic properties. Once this control mechanism has been perfected, it should also help to reduce air pollution and noise emission, decrease a fuel burn and increase the overall performance of rotorcraft. These benefits would be achieved by allowing rotorcraft to operate at a wider range of rotor speeds as opposed to the current state-of-the-art designs where the rotor speed is almost constant in order to avoid potentially harmful resonances of the blades [2]. This concept was already introduced in [3–5], but many of its aspects have not yet been fully addressed and experimentally validated.

Tendons or other means of applying compressive axial loading have already been used in a number of applications, often as actuators or a means of vibration control. A comprehensive review of active cable and tendon control can be found in [1, 6]. From a number of studies that utilised tendons, a few used a similar configuration to the present one, i.e. a beam-like structure loaded by a tendon. For example, in [7, 8] a tendon was used for vibration control of a simple cantilever beam. It was found that vibration energy of the beam in a prescribed frequency range can be removed by applying and releasing the tension in a specific manner, thereby effectively suppressing the vibration of the beam. These studies mainly focused on the control aspects of the problem, but the modelling of the dynamic response was also performed using the Euler-Bernoulli beam theory and the presence of the tendon was accounted for by an axial force. The same approach of modelling a beam-cable system was also employed in [9] with the difference that the tendon was

made of a shape-memory alloy. It was shown therein that in addition to the vibration suppression by means of an active control, a significant amount of damping can be introduced to the system by the tendon. In the previous studies, simple beam models with an axial force were considered, partly because the dynamics of such axially-loaded beams has been well understood [10]. In contrast, the use of cable that is mounted inside a helicopter tail boom for response suppression was numerically and experimentally investigated in [11]. Unlike in the previous studies, the system was modelled using the finite element method. It was shown that the cable can be tuned as a active vibration absorber which not only positions an antiresonance at the excitation frequency for a critical location on the primary structure, but also shifts the natural frequencies of the system. The interaction between the primary structure and the cable in terms of eigenvalue curve veering was also observed.

The present paper deals with the dynamic analysis of the beam-tendon system which is an idealisation of the active tendon concept whose development motivates this study. The present paper extends [3] by considering the bending-torsion coupling of the primary beam and using a more sophisticated model of the tendon. To the best knowledge of the authors, the same means of modelling has not yet been reported in literature. The paper is organised as follows: in section 2 the mathematical model of the beam-tendon system and the numerical approach used to obtain the modal properties are introduced. Then, the experimental set-up is described in section 3 and the computed results are compared to the experimental ones. In section 4 it is briefly shown how the presence of the tendon modifies the rotor properties of the Bo105 helicopter. Lastly, the discussion and future challenges are given in section 5.

2 Modelling approach

The system under consideration is a rotating straight cantilever beam with a cross-section which has one axis of symmetry (therefore featuring bending-torsion coupling) and is axially loaded by a tendon. The tendon is attached to the beam's tip, passes through its whole body (parallel to the neutral axis) and is fixed at the same location as the beam. The tendon can be placed in any location on the axis of symmetry of the cross-section. A tip mass which serves as a tendon attachment point is located at the free end of the beam (see the experimental set-up in Fig. 1 for detail).

The beam is modelled by means of the Houbolt-Brooks equations [12] which were modified to include the effect of the tendon-induced axial force while the tendon is modelled using the wave equations [13] augmented by the effects of centrifugal forces. The blade and tendon are coupled via the boundary conditions at the tip (free end). At the root, both are fixed so their displacements are equal to zero. At the tip, the displacement of both are identical and the tendon-induced axial force contributes to the shear and moment conditions of the blade. Since the tendon is free to vibrate inside the blade, no other connectivity conditions were enforced.

A set of partial differential equations (PDEs) describing the blade with the tendon can be written as (the terms that are not included in the original Houbolt-Brook equations [12] are underlined and the pre-twist $\beta(x)$ is equal to zero)

$$\left(EI_1 w'' - Te_A\phi + \underline{Pe_P\phi}\right)'' - \left(Tw' - \underline{Pw'} + \Omega^2 mxe\phi\right)' + m(\ddot{w} + e\ddot{\phi}) = 0, \tag{1a}$$

$$\left(EI_2 v''\right)'' - \left(Tv' - \underline{Pv'}\right)' + m(\ddot{v} - \Omega^2 v) = 0, \tag{1b}$$

$$\begin{aligned}\left(\left[-GJ - Tk_A^2 + \underline{Pk_A^2}\right]\phi'\right)' - (Te_A - \underline{Pe_P})w'' + \underline{P(e-e_P)\beta_y\phi''} \\ + \Omega^2 m\left(xew' + \left[k_{m2}^2 - k_{m1}^2\right]\phi\right) + m(k_m^2\ddot{\phi} + e\ddot{w}) = 0,\end{aligned} \tag{1c}$$

$$Pw_{\mathrm{t}}'' - \left(T_{\mathrm{t}} w_{\mathrm{t}}'\right)' - m_{\mathrm{t}}\ddot{w}_{\mathrm{t}} = 0, \tag{1d}$$

$$Pv_{\mathrm{t}}'' - \left(T_{\mathrm{t}} v_{\mathrm{t}}'\right)' - m_{\mathrm{t}}\left(\ddot{v}_{\mathrm{t}} - \Omega^2 v_{\mathrm{t}}\right) = 0, \tag{1e}$$

where $(\dot{\bullet})$ and $(\bullet)'$ are time and spatial partial derivatives, respectively, $w(t,x), v(t,x)$ are, respectively, flapping (out-of-plane of rotation) and lead-lag (in-plane of rotation) bending displacements of the beam, $\phi(t,x)$ is a torsional displacement, x is the independent spatial variable measured along initial position of the elastic axis ($0 \leq x \leq R$), R is the length of the beam, t is time, EI_1 and EI_2 are the flapping and lead-lag rigidity, respectively, GJ is the torsional rigidity, e_A is the distance between tensile and elastic axes, e is the distance between mass and elastic axes, Ω is the angular velocity of rotation, m is the mass of the beam per unit length, k_A is the polar radius of gyration of cross-sectional area, k_{m1} and k_{m2} are the polar radii of gyration, k_m is the polar radius of gyration of cross-sectional mass about elastic axis, β_y is a cross-sectional parameter, $w_\mathrm{t}(t,x), v_\mathrm{t}(t,x)$ are flapping and lead-lag transversal displacements of the tendon, respectively, P is the applied tension (always positive) of the tendon, m_t is the mass of the tendon per unit length, and e_P determines the position of the tendon. If $e_P = 0$ the tendon coincides with the elastic axis whereas for $e_P = e$ with the mass axis. The centrifugal forces acting on the beam and the tendon are given by

$$T = \Omega^2 \int_x^R m\hat{x}\,\mathrm{d}\hat{x}, \qquad T_\mathrm{t} = \Omega^2 \int_x^R m_\mathrm{t}\hat{x}\,\mathrm{d}\hat{x}, \tag{2}$$

Equations (1a)-(1c) are the modified Houbolt-Brooks equations which include the tendon-induced axial force P. Since these equations are based on the Euler-Bernoulli theory, which neglects the transverse shear deformation, rotary inertia effects and warping, an infinitely rigid planar cross-section that remains planar and normal to the elastic axis after the deformation is assumed [14]. Equations (1d) and (1e) are the wave equations describing the motion of the tendon under the assumption that its cross-sectional area remains unchanged during deformation (the Poisson's effect is not included) [13].

The PDEs are accompanied by an appropriate set of boundary conditions (BCs) which ensure the coupling between the tendon and the beam at the tip. The boundary conditions at the fixed end (for $x = 0$) are

$$v = w = \phi = v' = w' = w_\mathrm{t} = v_\mathrm{t} = 0, \tag{3}$$

and at the free end (for $x = R$)

$$Q = 0 = (GJ - \underline{P(e - e_P)\beta_y - Pk_A^2})\phi', \tag{4a}$$

$$M_y = 0 = EI_1 w'', \tag{4b}$$

$$M_z = 0 = EI_2 v'' + \underline{Pe_P}, \tag{4c}$$

$$V_z = 0 = -M_y' + m_\mathrm{tip}\ddot{w} - \underline{Pw'} + \Omega^2 mex\phi + \underline{Pw_\mathrm{t}'}, \tag{4d}$$

$$V_y = 0 = -M_z' + m_\mathrm{tip}\ddot{v} - \underline{Pv'} + \Omega^2 mex + \underline{Pv_\mathrm{t}'}, \tag{4e}$$

$$w_\mathrm{t} = w + e_P\phi, \tag{4f}$$

$$v_\mathrm{t} = v + e_P, \tag{4g}$$

where m_tip is the mass located at the tip. Equation (3) prescribes zero displacements and slopes of the blade, and zero displacements of the tendon at the fixed end. Equations (4a)-(4c) prescribe zero torque and moments (including the moments induced by the tendon) at the tip of the blade. The blade is coupled with the tendon through the shear boundary conditions (Eqs. (4d) and (4e)), and the displacement equality at the tip enforced by Eqs. (4f) and (4g). The tip mass, characterised by m_tip, also contributes to the shear boundary conditions at the tip.

It should be noted that while the rotating beam-tendon system has not yet been studied in literature, a beam featuring the bending-torsion coupling loaded by an axial force placed in an arbitrary position of the cross-section has been previously considered. In particular, in [15,16] a system of equations describing such beam, albeit without inertial forces ($m = 0$), was used to analyse its structural stability. The same set of equations, augmented by the inertial forces ($m \neq 0$), was also used in [17] to investigate the response to deterministic

and random excitation. The PDEs introduced in Eqs. (1a)-(1c) reduce to the equations used in [17] when the centrifugal force T is removed, and to the equations used in [15, 16] for $m = 0$.

In order to evaluate the modal properties (natural frequencies and mode shapes) of the beam-tendon system, an assumption of the normal mode is used. A solution of any given dependent variable is expressed as the multiplication of the time-invariant mode shape and the time-varying harmonic function of the constant frequency in the following form

$$\begin{gathered} w(t,x) = W(x)\mathrm{e}^{\mathrm{i}\omega t}, \quad v(t,x) = V(x)\mathrm{e}^{\mathrm{i}\omega t}, \quad \phi(t,x) = \phi(x)\mathrm{e}^{\mathrm{i}\omega t}, \\ w_{\mathrm{t}}(t,x) = W_{\mathrm{t}}(x)\mathrm{e}^{\mathrm{i}\omega t}, \quad v_{\mathrm{t}}(t,x) = V_{\mathrm{t}}(x)\mathrm{e}^{\mathrm{i}\omega t}. \end{gathered} \tag{5}$$

Substituting the normal mode forms into Eqs. (1) and (4) allows one to eliminate time and rewrite the PDEs into a system of first order ordinary differential equations (ODEs) that, together with the BCs, define a boundary value problem. This boundary value problem can then be solved by a Matlab bvp4c solver [18] for unknown natural frequencies ω and corresponding mode shapes $W(x)$, $V(x)$, $\phi(x)$, $W_{\mathrm{t}}(x)$ and $V_{\mathrm{t}}(x)$. This solver is very versatile since it uses a collocation method but may suffer from a decreased numerical performance if an appropriate starting guess is not provided.

3 Experimental validation

In this section, the theoretical model is validated using a bench-top experiment. A similar experiment has been already presented in [3], where the pure bending of an Euler-Bernoulli beam loaded by a tendon has been considered.

3.1 Experimental set-up description

The picture of the bench-top experiment can be seen in Fig. 1. The beam (whose properties are detailed in section 3.2) is rigidly clamped at one and free at the other end. The tendon is attached to the tip mass mounted at the free end of the beam, and passes freely inside the beam towards the clamp where its flexural motion is constrained. The tendon then continues through the clamp and pulley and is attached to a hanging platform. The tension of the tendon, and hence the axial load applied to the beam, is controlled by the amount of mass placed on the platform. The tendon can be attached in several discrete positions along the cross-sectional axis. Two notable positions, i.e. the mass and elastic axis, that are further discussed in this paper are marked in the inset in Fig. 1. The applied tension and the placement of the tendon will be shown to have an influence on the dynamic response of the system.

The beam is excited using a modal shaker to obtain frequency response functions (FRFs). A shaker was preferred to a modal hammer because of the repeatability that is required due to a large number of measurements needed to validate the theoretical model for a wide range of loading cases. Moreover, it was also observed in [3] that few tendon-dominated modes can be excited using a modal hammer. The shaker was controlled via a modular control and data acquisition (DAQ) system. Random excitation, which linearises possible weak non-linearities, such as the friction between the tendon attachment and the tip mass, was used to excite the frequency range between 5 and 400 Hz. The response data were collected from the tip using two small uni-directional accelerometers placed perpendicularly to each other. A higher number of accelerometers was not used because it was found that their combined mass had a significant disturbing influence on the modal properties of the beam. The laser displayed in Fig. 1 was not used in this study.

The response data and the input force were used to estimate the FRFs using the H_v-estimator [19] for the all considered load cases. The load was varied using the weight plates in one kilogram increments from 1 kg to 44 kg. The natural frequencies (damping and mode shapes are not discussed in this paper) were estimated using the least-square complex frequency (LSCF) estimator [20].

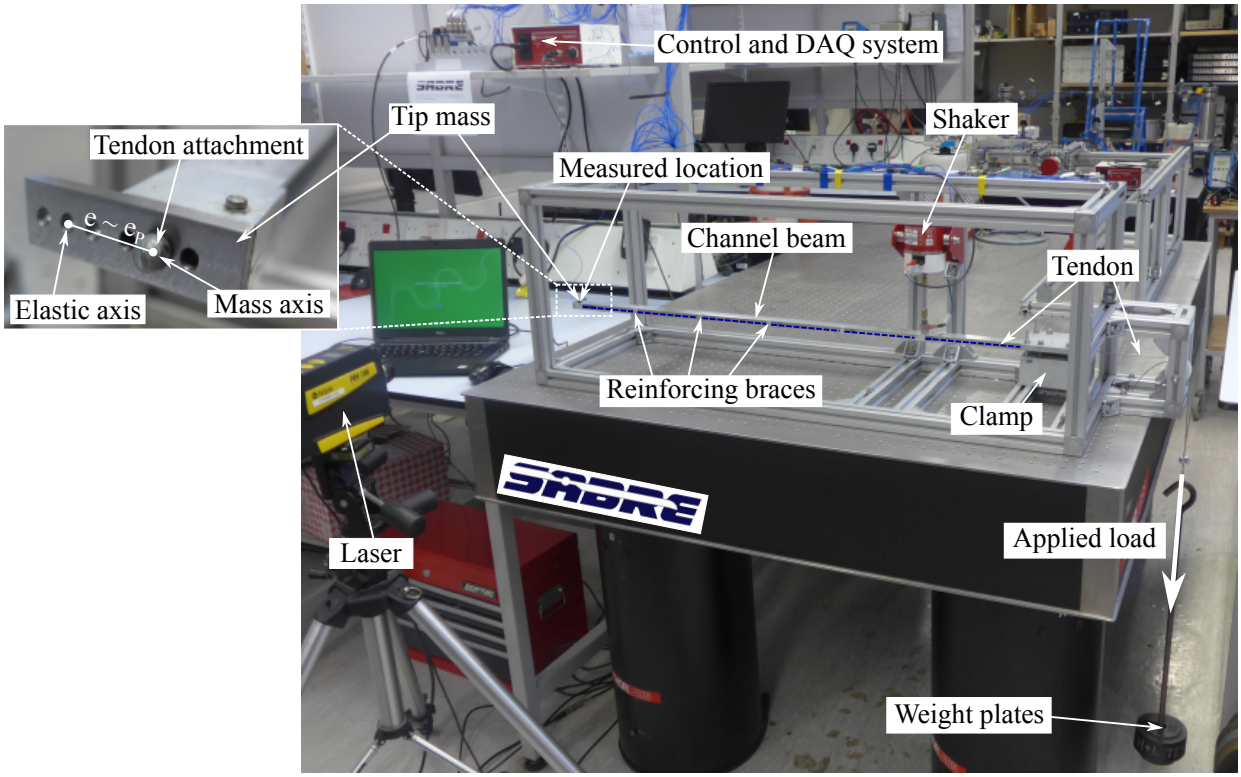

Figure 1: Experimental set-up. The cantilever beam subjected to the tendon-induced axial force generated by the applied load is excited by a shaker to obtain the frequency response functions for the estimation of modal properties which are then used to validate the theoretical model.

3.2 Nominal channel beam and tendon properties

A beam with the channel cross-section, which was reinforced by several braces (see Fig. 1), was used to validate the theoretical model. The selection of this beam was a compromise based on the following criteria which were proposed to ensure that the effect of the tendon is observable while the beam is a representative idealisation of a rotorcraft blade:

- *Bending-torsion coupling* - most modern rotocraft blades exhibit a certain amount of bending-torsion coupling. This coupling is introduced due to their design and the use of composite material. In the present study, the beam was made of aluminium, so the coupling was introduced through the choice of the cross-sectional geometry.
- *The number of modes* - the number and character of the vibration modes (flapping, lead-lag, torsional or coupled) should be similar to a typical rotorcraft blade. For the Bo105 helicopter studied in section 4 there are 10 modes between 5 Hz and 450 Hz. The experimental beam was designed in such a way that it has similar number and character of modes in a comparable frequency range. This was achieved by the choice of the material (aluminium) and geometry of the beam.
- *The effect of the tendon* - The tendon should produce observable effects in the investigated loading range. In particular, the reduction of the natural frequency for the first two modes should be at least 5 % of their nominal values. In order to achieve such reduction, the rigidity of the beam was lowered by using a thin-walled profile.
- *Boundary conditions* - a typical hingeless rotorcraft blade is fixed at the root and free at the other end. In addition, a tip mass is often used to improve the overall performance, vibration and acoustics of helicopters [21]. Therefore, a cantilever beam with a tip mass (which acts as an attachment point for the tendon) was used.

- *Euler-Bernoulli theory* - The theoretical model was derived based on the Euler-Bernoulli theory which neglects the transverse shear deformation, rotary inertia effects and sectional warping. Therefore, the experimental beam should be in line with the idealisation used. However, due to the previous requirements (open, thin-walled profile needed to emphasise the tendon effects and bending-torsion coupling), the assumptions of the Euler-Bernoulli theory would be violated. Therefore, it was attempted to reinforce the beam with several braces to minimise the influence of the neglected effects.

The nominal properties of the beam seen in Fig. 1 are $R = 1\,\mathrm{m}$, $A = 9.47 \times 10^{-5}\,\mathrm{m}^2$, $EI_1 = 169.30\,\mathrm{N\,m}^2$, $EI_2 = 354.26\,\mathrm{N\,m}^2$, $GJ = 2.42\,\mathrm{N\,m}^2$ and $e = 0.0191\,\mathrm{m}$. The beam was weighted and the mass was found to be $m = 0.2478\,\mathrm{kg\,m}^{-1}$. Likewise, the mass of the tip is $m_{tip} = 0.0269\,\mathrm{kg}$. Other parameters can be computed from the above parameters in a standard manner as outlined in [12, 22]. The tendon is made of a steel wire with $m_\mathrm{t} = 0.0125\,\mathrm{kg\,m}^{-1}$.

3.3 Validation of the theoretical model without the tendon

Before including the tendon into the experiment, the model of the beam with and without the tip mass was validated. The purpose of this step was to obtain the underlying model of the beam, which is defined using Eqs. (1a)-(1c) without the axial force P, as accurately as possible so that the effect of the tendon can be studied separately.

Firstly, the beam without the tip mass is considered. The comparison of the experimental and computed nominal natural frequencies can be found in Fig. 2. It can be seen in Fig. 2(c) that the relative error of almost all modes is greater than 5 % with the greatest error over 15 % for 3rd lead-lag (3L-L) mode. Therefore, it was

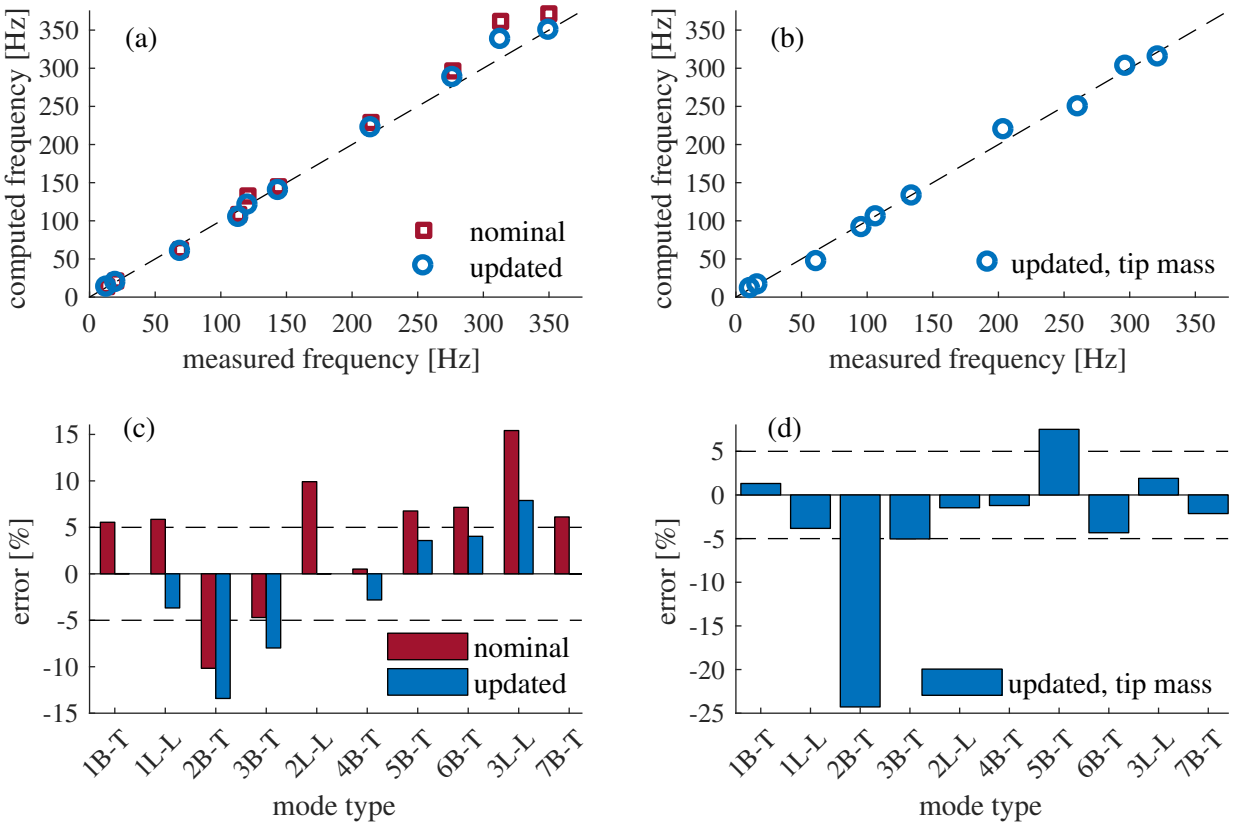

Figure 2: Comparison of experimental and computed natural frequencies without the tendon: (a) no tip mass, (b) with tip mass, (c) error for no tip mass, and (d) error with the tip mass. xB-T means the x$^{\mathrm{th}}$ mode dominated by the bending-torsion motion, whereas xL-L is the x$^{\mathrm{th}}$ lead-lag mode.

decided to update selected model parameters such that the difference between the two sets of frequencies is minimised. The updating was performed using a single-objective multi-variable optimisation using a genetic algorithm [23], whereby the objective function was defined by the error between the measured and computed natural frequencies. EI_1, EI_2 and GJ were selected for the optimisation since the natural frequencies are the most sensitive to these three parameters and their uncertainty.

The optimised bending and torsional rigidities, EI_1, EI_2 and GJ, were 89.11 %, 82.79 % and 95.54 % of their nominal values, respectively. The resulting natural frequencies and their comparison with the experimental values can be seen again in Fig. 2(a) and (c). Although the nominal parameters have not been dramatically changed, the overall character of the error between the measured and updated frequencies is very different. The error of almost all modes has decreased under the 5 % threshold. Unfortunately, the error of the 3$^{\text{rd}}$ and 4$^{\text{th}}$ mode has increased while the error of the 9$^{\text{th}}$ mode (3L-L) decreased but remained higher than 5 %. It is believed that if more parameters were used for the optimisation the resulting error would be lowered. However, more parameters have not been used to avoid creating an artificial model matching the limited set of experimental results. Moreover, it is also possible that the model used cannot accurately represent the experimental beam due to the Euler-Bernoulli theory assumptions violation. This assertion will be supported in section 3.4 where it is shown that the error is intrinsic to the model of the beam without the tendon and therefore has negligible effects on the model with the tendon.

Having the parameters of the model for the beam without the tip mass updated, these parameters were used to compute the natural frequencies of the model with the tip mass. The experimental and computed results are again compared in Fig. 2(b) and (d). No additional updating was performed because the tip mass could be easily measured. As expected, the magnitude of all natural frequencies reduced when the tip mass was added. When compared to the experiment, it can be seen that the error of some modes even decreased. Unfortunately, the error of the 3$^{\text{rd}}$ mode increased significantly, approaching 25 % and the error of 7$^{\text{th}}$ mode (5B-T) has also exceeded 5 %. The errors of all other modes are lower than 5 % which is herein considered as an acceptable error which can be explained by the violations of the Euler-Bernoulli theory assumptions used in the theoretical model.

3.4 Validation of the theoretical model with the tendon

The Campbell diagram, which shows the dependence of the natural frequencies on the applied load, is obtained for the case when the tendon coincides with the mass axis can be seen in Fig. 3. Two sets of frequency loci can be distinguished in both the numerical and experimental data. There are ten beam-dominated modes present which decrease very slowly with the increasing load (this effect is better seen in Fig. 5). It can also be noticed that for very low applied load, these frequency loci are very close to those obtained for the beam without the tendon. The other modes, which increase rapidly with the added masses, are the tendon-dominated modes. Experimentally, seven of such modes were captured. However, there would be many more for very low loading. Such modes have not been sufficiently excited in the experiment and even numerically, they were not obtained. The inability of the solution method to find the higher modes for low loading seems to be caused by the need to provide extremely accurate starting guess. Unfortunately, due to a very large number of modes it is very difficult to find such a starting guess that would lead to all the modes. The beam-dominated and tendon-dominated modes interact with each other through mode veering. The number of veering regions is very high for the higher frequency regions and lower loading due to the large number of the tendon-dominated modes in that region. A selected veering region is shown in Fig. 6 and discussed in more detail in section 3.6.

Overall, the agreement between the experiment and theoretical results is deemed to be satisfactory. In particular, the rapidly increasing tendon-dominated modes match the measured values very well. The computed and experimentally measured beam-dominated modes exhibit the same trends with systematic discrepancies manifested as frequency offsets. In order to explain the offsets and to emphasize the effect of the tendon, four loading configurations are studied in Fig. 4 (for applied load equal to 1, 15, 30 and 44 kg).

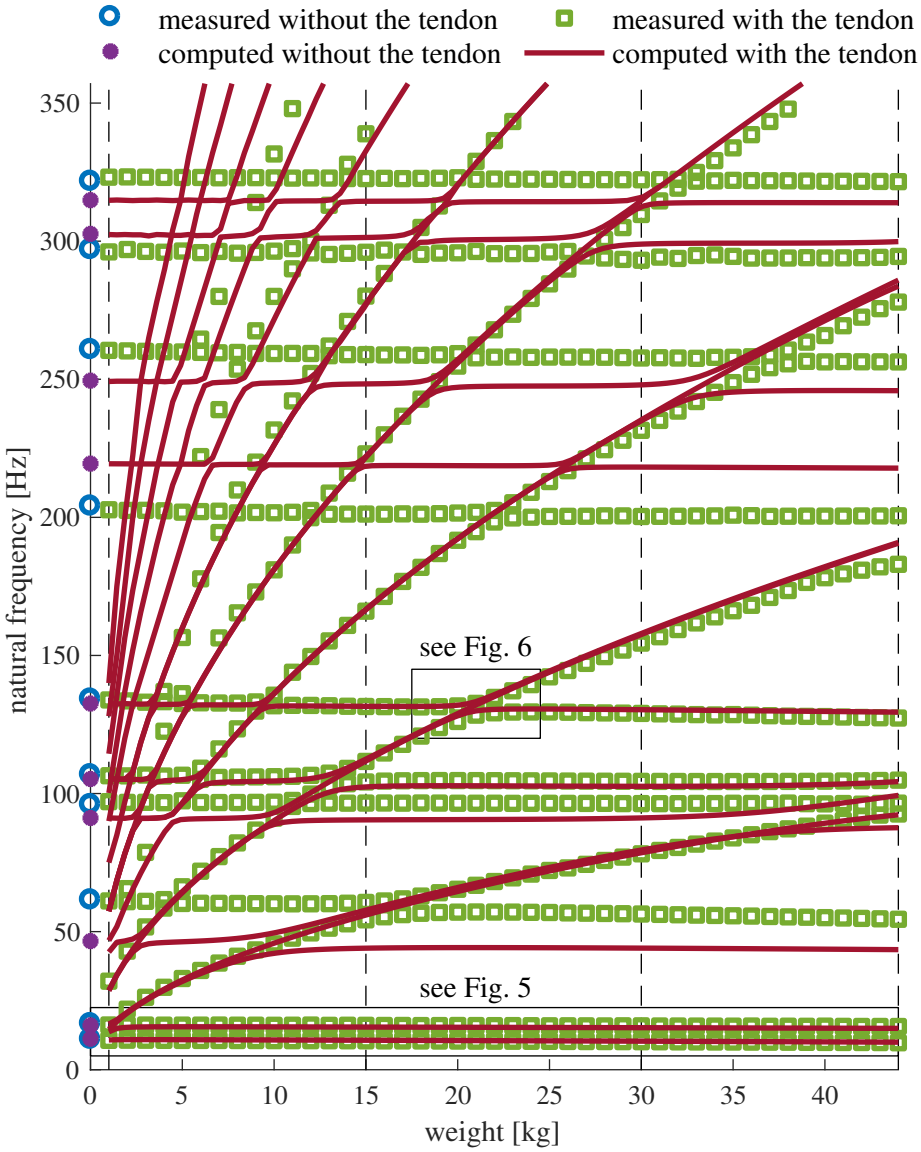

Figure 3: Comparison of the computed and measured Campbell diagrams. Rapidly increasing natural frequencies belong to the tendon-dominated modes while almost constant frequency loci belong to the beam-dominated modes.

The reduction of the natural frequency caused by the tendon is shown in Fig. 4(a). It can be seen that for almost all captured modes, the frequency decreases with the increased applied load. In addition, the reduction is much higher for the first mode (over 10 %) than for the rest of the modes. Some of the values for the first three modes could not have been obtained (n/a in Fig. 4) because of the presence of veering in the Campbell diagram (see Fig. 5 for detail of the first mode). While the reduction of the natural frequency depends on the applied load, the errors between the experimental and computed values stay almost constant with increasing load as evidenced by Fig. 4(b). A small variance of these errors can be explained by the standard experimental errors.The error for the beam with the tip mass but without the tendon (from Fig. 2(d)) is shown Fig. 4(b) in blue in order to demonstrate that the error for different loads cases is not only constant, but also comparable to the error for the beam without the tendon. Since the error is invariant with the applied load while the anticipated reduction of the natural frequency is observed, it can be concluded that the effect of the tendon was captured correctly by the model. This also supports the previous assertion that the error in Fig. 2(d) and the offset in the frequency loci in Fig. 3 is caused solely by the errors associated with the modelling of the beam using the Euler-Bernoulli theory.

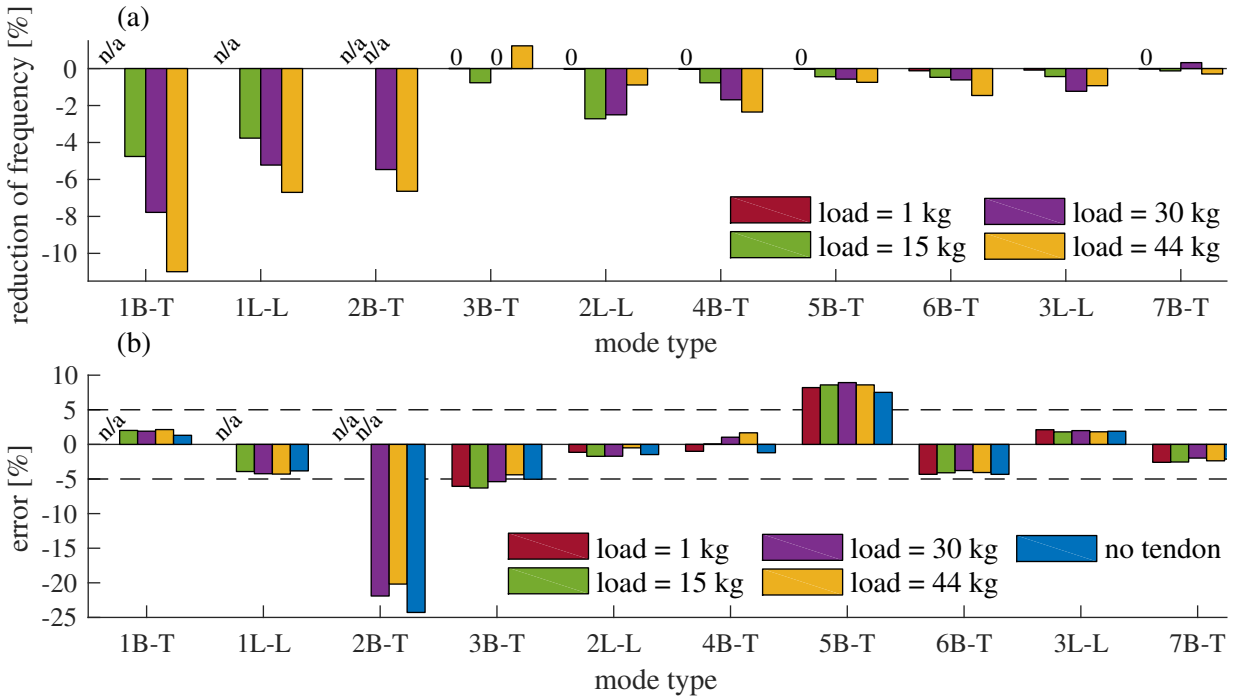

Figure 4: The effect of the tendon for the four loading configurations: (a) reduction of the natural frequency and (b) error between the measured and computed frequencies. The missing values could not be obtained due to the presence of veering.

3.5 The effect of the position of the tendon

All the results presented so far were obtained for the case where the tendon coincides with the mass axis of the beam, as depicted in the inset of Fig. 1. Figure 5 compares the previous results with the results obtained, both computationally and experimentally, for the tendon placed in the elastic axis. It can be seen that the position of the tendon has an influence on the natural frequencies of the beam-dominated modes. The computed results correspond to the experimental values qualitatively quite well although there are quantitative differences. These differences, however, correspond to the error that is intrinsic to the model of the beam as discussed in section 3.4. The results indicate that the higher reduction of the frequency can be achieved by placing the tendon in the mass axis. This is in line with the conclusions of stability analysis made in [15, 16] that the critical load is at its maximum when the axial force coincides with the elastic axis.

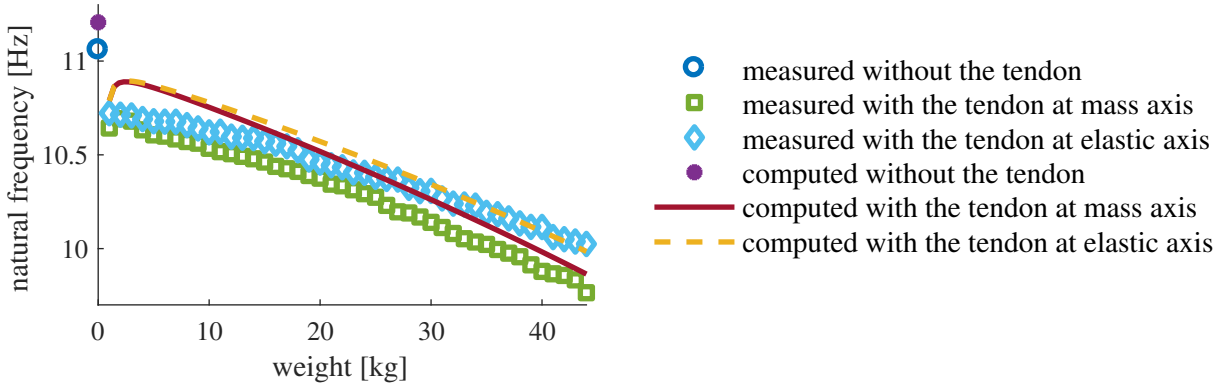

Figure 5: Comparison of experimental and computed natural frequencies of the first flapping mode with the tendon placed in either mass or elastic axis

Although it is reasonable to expect that the measured frequencies produce smooth trends with increasing loads, some small deviations can be observed in Fig. 5. These deviations are very small (not exceeding 0.1 Hz) and can be explained by the presence of the standard experimental errors. It is believed that these small deviations caused a variance of the error shown in Fig. 4(b) which would be otherwise constant. Furthermore, Fig. 5 also shows why some of the values in Fig. 4 were not evaluated. Specifically, for the load equal to 1 kg it would be meaningless to compare the computed and measured frequencies, because the computed values are influenced by veering caused by the tendon modes that have not been excited in the experiment.

3.6 The veering in the beam-tendon system

In Fig. 3 a number of veering regions can be seen, one of which is enlarged in Fig. 6. The computed modes are also added to illustrate the veering. Typical signs of veering can be observed - two modes converge, but then suddenly diverge and continue on the trajectory of the other mode while swapping all their properties including the damping ratio and mode shapes. It can be seen that the mode shape in inset 1a became the mode shape in inset 3c which is located at the different frequency locus. Similarly, the mode shape in 3a swapped with that in 1c. The frequency curve which passes through the veering regions unchanged is associated with the motion of the tendon in the lead-lag direction. Since this motion is not coupled to bending-torsion vibration of the beam, it is not influenced by the veering as also evidenced by the mode shapes in insets 2a-2c. A similar phenomenon was also observed in [11] for a symmetric cable where it raised concerns with regards to the application of the tuned vibration absorber developed therein. The veering is a frequent and important phenomenon occurring in the studied beam-tendon system as seen in Fig. 3 and will be therefore studied closely in the future.

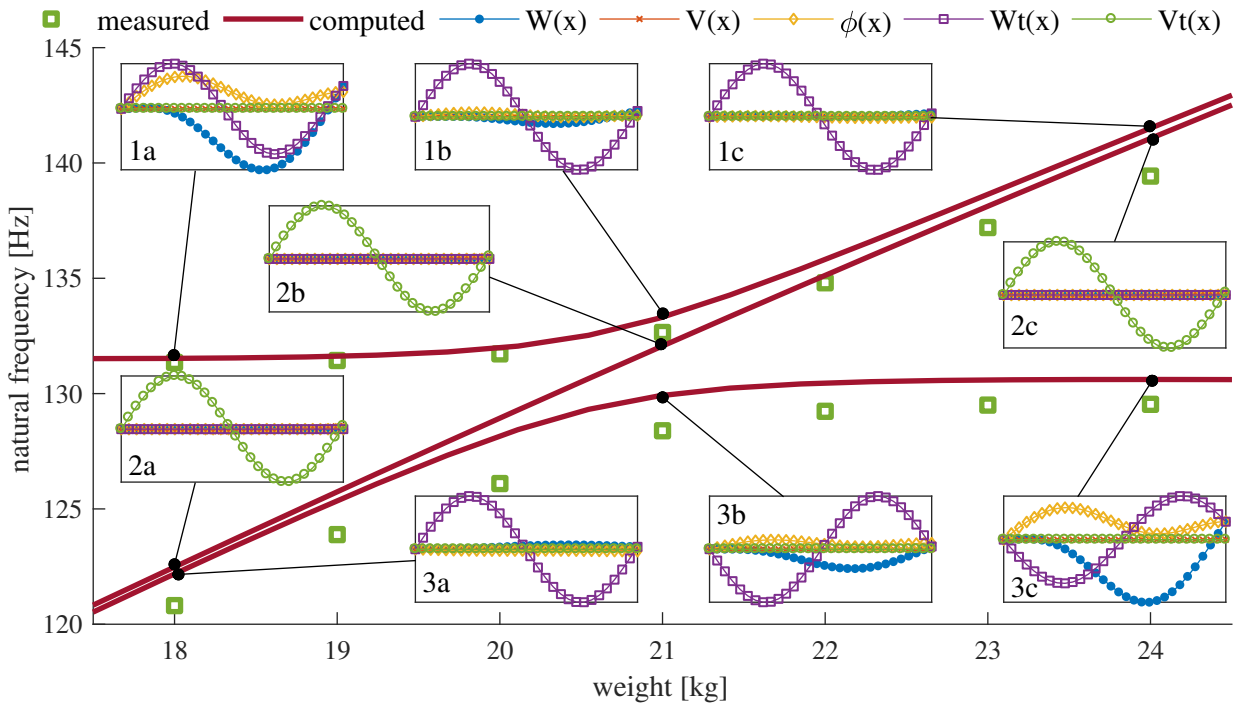

Figure 6: Veering in the beam-tendon system. The mode shapes displayed have been obtained numerically.

4 A helicopter case study

This section describes an application of the tendon as a means of manipulating the dynamic properties of a helicopter rotor blade, highlighting its benefits and potential as well as future challenges that will have to be addressed.

4.1 Selected helicopter and rotor description

The selected helicopter is the Bo105, currently produced by Airbus Helicopters. The Bo105 is a light, widely used, multi-purpose helicopter deployed in medical services, police, search and rescue, and military missions. This helicopter was selected as its rotor blade structural and airfoil aerodynamic data are well defined, and because this helicopter is used a reference aircraft in SABRE project [5].

The Bo105 features a four-bladed hingeless main rotor and a two-bladed teetering tail rotor. The main rotor blade is used in this study since it is more suitable for the application of the proposed control mechanism. The equivalent uniform structural properties of each Bo105 blade are $R = 4.912\,\mathrm{m}$, $EI_1 = 10\,000\,\mathrm{N\,m^2}$, $EI_2 = 170\,000\,\mathrm{N\,m^2}$, $GJ = 4850\,\mathrm{N\,m^2}$, $m = 5.5\,\mathrm{kg\,m^{-1}}$, $k_{m1} = 0.090\,\mathrm{m}$, $k_{m2} = 0.0648\,\mathrm{m}$, $e = -0.01\,\mathrm{m}$, $e_A = 0\,\mathrm{m}$, $k_A = 0.041\,\mathrm{m}$ and $m_{\mathrm{tip}} = 0\,\mathrm{kg}$. Since the blades have initial linear pre-twist characterised by $\beta(x) = -0.022x + 0.0663\,\mathrm{rad}$, this pre-twist was also considered in Eq. (1) in the same way as in [12]. The Bo105 helicopter operates with the reference (nominal) rotor speed $\Omega_{\mathrm{ref}} = 44.4\,\mathrm{rad\,s^{-1}}$. For the purpose of this study, a nylon rope with $m_{\mathrm{t}} = 0.0887\,\mathrm{kg\,m^{-1}}$ is used as a tendon and the reference tendon tension was chosen to be $P_{\mathrm{ref}} = 5250\,\mathrm{N}$.

4.2 Selected results for the helicopter case study

The comparison of the baseline and modified frequency diagrams can be seen in Fig. 7(a). The blue solid frequency loci represent the response of the baseline rotor with nominal parameters where the first ten modes are considered, and the rotor speed is varied between 0 and 1.2 of the reference rotor speed Ω_{ref}. It might appear that the dynamic behaviour of the rotor has been significantly changed by the tendon since many new modes and veering regions, especially at higher frequencies, have emerged (red dashed lines). However, after a close examination of the frequency diagram and related mode shapes (not shown), it can be found that all new loci are related to modes that are dominated by the motion of the tendon and do not therefore have a significant influence on the blade's dynamics. However, the tendon does influence the blade-dominated modes by reducing their frequency and by creating a number of veering regions. The former is at the moment seen as the key effect of the tendon that can be utilised to control the dynamic behaviour of the rotor.

It can be noticed in Fig. 7(a) that there is a major difference between the behaviour of the blade- and tendon-dominated modes. While the blade-dominated modes increase with the increasing rotor speed due to the centrifugal effects, the tendon-dominated modes decrease. This is caused by the fact that the tendon, which is modelled as a taut string, loses its tension due to the applied centrifugal force which leads to the rapid decrease of its natural frequencies. The preceding observation indicates that should the tendon have a desired effect, i.e. to influence the dynamic behaviour of the blade-dominated modes by shifting their frequencies, the applied tension must be higher than the centrifugal force at that rotor speed. To meet this requirement, the tendon tension must be actively controlled based on the variations in the rotor speed and other flying conditions. Otherwise, the tendon-induced axial load could cause stability issues at the low rotor speeds while having little effect at the operational ones. Such situation is depicted in Fig. 7(a) as well - while the reduction of the first blade-dominated mode at the reference rotor speed is relatively minor, the same tendon tension led to a complete disappearance of the first mode at the low rotor speed. The first mode emerges at 0.1 of the reference rotor speed. Such behaviour can potentially lead to the loss of stability and is therefore one of the reasons why the active control of the tendon tension may be of paramount importance in the future.

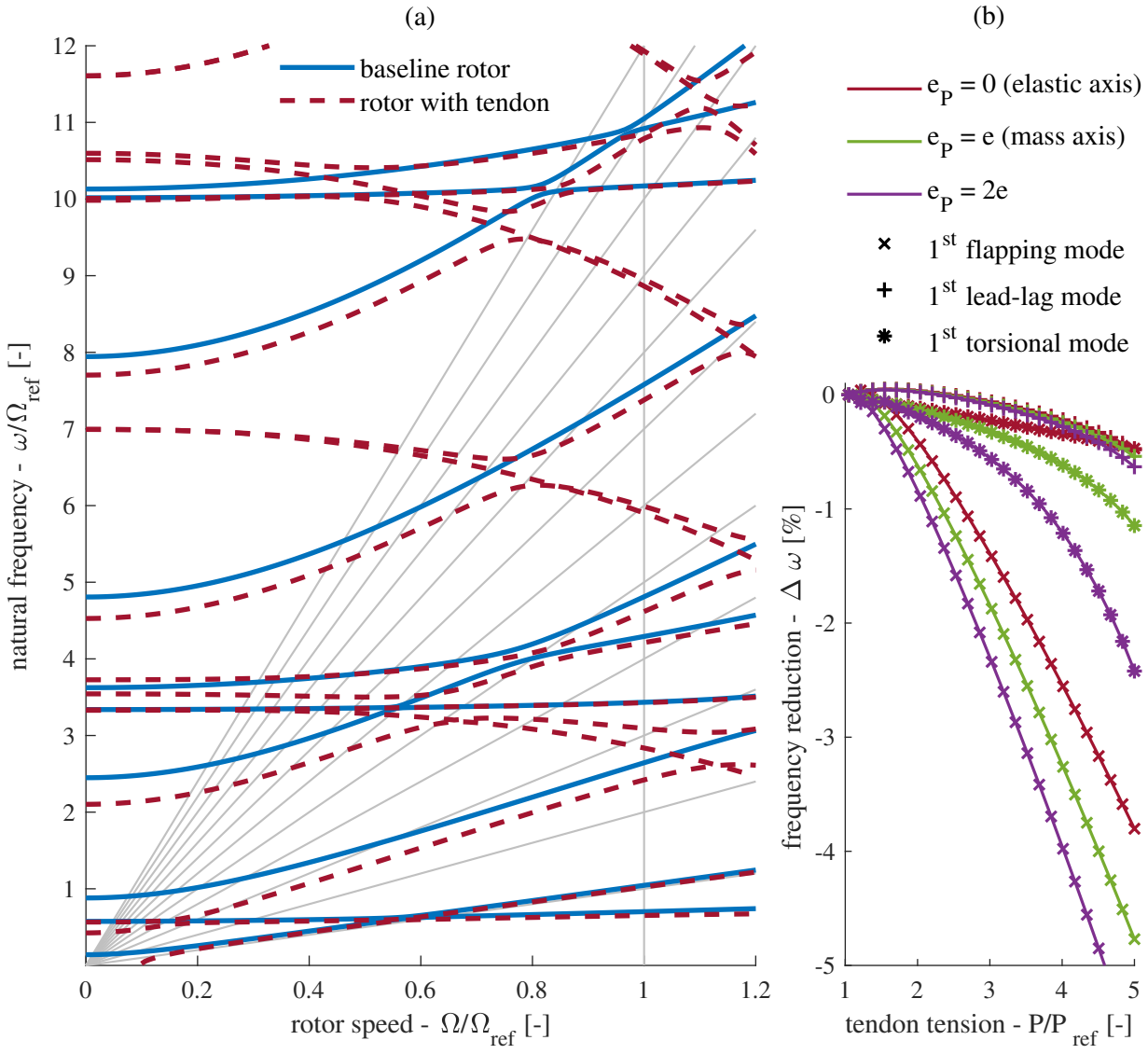

Figure 7: A case study of the Bo105 helicopter rotor blade with the tendon: (a) the comparison of the baseline and modified frequency diagrams and (b) the relative frequency reduction at reference rotor speed evaluated for three different positions of the tendon within the blade and a range of tendon tensions

The dependence of the relative frequency reduction on the applied tension and the position of the tendon in the blade is shown in Fig. 7(b). Three different tendon positions have been considered - the tendon coincides either with the elastic axis, mass axis or further behind the mass axis. It is seen that by increasing the applied tension, the frequency reduction is increased as well. However, similar to the experiment this reduction is not the same for all modes. For example, the frequency of the first flapping mode was reduced more than the lead-lag one, which is in line with the experimental observation in Fig. 4. The position of the tendon also has a considerable effect. In particular, the torsion-dominated mode is significantly influenced. While the frequency of this mode reduces linearity in the investigated range of tension when the tendon coincides with the elastic axis, the reduction is approximately quadratic when the tendon lies elsewhere. Moreover, it seems that increasing the offset of the tendon from the elastic axis leads to a more substantial reduction of the natural frequency of the torsional mode. Therefore, to achieve the optimal performance of the active tendon in the future, not only the tendon tension must be controlled, but also the position of the tendon in the airfoil must be considered.

5 Discussion

In previous sections, the theoretical model of the rotating beam-tendon system has been introduced, its experimental validation has been conducted and a case study on the Bo105 helicopter has been presented. In this section, the main findings, assumptions and limitations are discussed, and directions for the future work are outlined.

The validation of the theoretical model given by Eq. (1) was conducted in section 3 using the natural frequencies. The validation was performed on the beam exhibiting the bending-torsion coupling which was meant to be a representative idealisation of a helicopter blade. In order to select the beam, a number of criteria, summarised in section 3.2, have been used. Unfortunately, while attempting to design the beam which would sufficiently demonstrate the tendon-induced effects, the assumptions of the Euler-Bernoulli theory were violated by selecting the thin-walled, open-section channel beam. Consequently, a good match was obtained only for the tendon-dominated modes, while, despite having the correct trends, the natural frequencies of the beam-dominated modes were offset from the measured ones. However, it was demonstrated using Fig. 2(d) and Fig. 4(b) that the offsets are the same for all loading configurations. Therefore, they are not caused by the tendon and merely originate from the violation of the Euler-Bernoulli assumptions. It can be therefore assumed that if the beam was modelled with a better accuracy, the overall agreement between the experimental and computational results would be improved.

It was found, both numerically and experimentally, that the tendon introduces two effects to the beam-tendon system. Firstly, it reduces the natural frequency of the beam-dominated modes and, secondly, it creates a number of veering regions. Both of these findings were also obtained in [3, 11], but the former was not observed in other studies [7–9] where only the latter effect was captured while modelling the tendon as an axial force. It was also observed that the position of the tendon inside the beam has an influence on the quantitative and qualitative reduction in the frequencies. In particular, the torsional modes seem to exhibit qualitative changes with the varying position of the tendon as shown in Fig. 7(b). However, reliable experimental results for the varying position of the tendon were unfortunately obtained for only the first mode, and, since no experimental results are available in literature, a general conclusion about the effect of the tendon position cannot yet be formulated. In particular, the effect of the position of the tendon on the torsional modes should be experimentally verified.

A number of assumptions have been considered to obtain the PDEs in Eq. (1) that describe the beam-tendon system. Most importantly, the Euler-Bernoulli theory was used. In order to facilitate this theory, the transverse shear deformation, rotary inertia effects and the sectional warping were neglected [14]. It is believed that the violation of these assumptions in the experimental set-up led to an inaccurate match with the experimental data despite an attempt to reinforce the experimental beam by the braces. The Euler-Bernoulli theory was used in this study to provide the first insights into the possibilities and challenges associated with the tendon. However, for the future development of the concept, especially with regards to its application in rotorcraft, a more general theory will have to be used. Although a large number of refined beam theories is available in literature [14], the composite beam theory appears to be the most general and widely accepted [24]. The use of the composite beam theory would be also preferable since the rotorcraft blades are usually made of composite materials, and the theory is able to capture all required effects, including warping and large deformation. The tendon was modelled as a taut string where it was assumed that its diameter remains constant [13]. Since a light-weighted tendon that would be suitable for the final application in rotorcraft will be most likely very compliant, its model will have to be adjusted. However, modelling the Poisson's effect in the wave equations renders the PDEs non-linear [13] and therefore unsuitable for the design studies. Similarly, any non-linearities (caused for example by joints, friction or large deformations) are currently not included in the analysis or experiment since their existence and importance are unknown.

The PDEs describing the beam-tendon system have been solved using a Matlab bvp4c solver [18] to obtain the modal properties. This solver is known to be very versatile, but requires a good starting guess to find all solutions in the frequency range of interest. In particular, it is very difficult to obtain the symmetric modes at the same natural frequency. The presence of the symmetric or almost-symmetric modes is, however, inherent

to the system so, in order to make the solution approach more robust, a method that does not require a starting guess should be used in further studies. Recently, a differential quadrature method (DQM) [25] has gained some popularity in structural dynamics, so its use will be considered for the present problem as well.

In section 4, a case study of the Bo105 helicopter was presented. From the results, it can be concluded that (i) the tendon can provide a means of reducing the natural frequencies of the blade-dominated modes, (ii) the control of the tension must be used to avoid not only potentially harmful resonances but also stability issues related to the tendon, (iii) the tendon position in the airfoil should be considered as a design variable and (iv) the veering caused by the varying tension and rotor speed should be further explored. Although the obtained results are encouraging, much work, such as a thorough consideration of aerodynamic stability issues, needs to be conducted before the concept can be commissioned. Nevertheless, the results of the case study highlighted the potential of the active tendon to provide a means of control required to adaptively avoid the harmful resonances at different operational conditions. This, possibly in conjunction with other morphing concepts [5], should enable rotocraft to operate over a wider range of rotor conditions, thereby increasing their efficiency and decreasing their fuel burn, air pollution and noise emission in the future.

6 Conclusion

This paper presented a numerical and experimental study of the coupled bending-torsion vibration of the tendon-loaded beam. The beam-tendon system was modelled using a set of partial differential equations and the free vibration analysis was performed using the collocation method. A test rig consisting of an open-section cantilever beam and the tendon that provides the axial load was used to experimentally validate the theoretical model. A satisfactory agreement between the numerical and experimental results was obtained and it was shown that the tendon not only reduces the natural frequencies of the beam, but also introduces frequency loci veering. Since the study was motivated by the future application of an active tendon in rotorcraft, the numerical model was augmented by considering the centrifugal effects and a case study performed on the Bo105 helicopter showed that the active tendon concept has potential to influence the rotor blade dynamic properties.

Acknowledgements

V. Ondra and B. Titurus would like to acknowledge the financial support of the European Community's Horizon 2020 Program provided through the project "Shape Adaptive Blades for Rotorcraft Efficiency (SABRE)", Grant Agreement 723491, and R. Dibble would like to thank The UK Vertical Lift Network and ESPRC for their support and funding.

References

[1] S. Korkmaz, *A review of active structural control: challenges for engineering informatics*, Computers and Structures, Vol. 89, No. 23-24 (2011), pp. 2113-2132.

[2] G.A. Misté, E. Benini, *Variable-speed rotor helicopters: performance comparison between continuously variable and fixed-ratio transmissions*, Journal of Aircraft, Vol. 53, No. 5 (2016), pp. 1189-1200.

[3] R.P. Dibble, B. Titurus, *Helicopter rotor blade modal tuning using internal preloads*, *Proceedings of International Seminar on Modal Analysis*, (2016).

[4] R.P. Dibble, B.K.S. Woods, B. Titurus, *Static aeroelastic response of a rotor blade under internal axial loading*, *Proceedings of European Rotorcraft Forum*, (2017).

[5] J. Rauleder, B.G. van der Wall, A. Abdelmoula, D. Komp, S. Kumar, V. Ondra, B. Titurus, B.K.S. Woods, *Aerodynamic rerformance of morphing blades and rotor systems*, *Proceedings of AHS International 74th Annual Forum & Technology Display*, (2018).

[6] A. Preumont, *Vibration Control of Active Structures: An Introduction*, Springer Netherlands (2012).

[7] S. Nudehi, R. Mukherjee, S.W. Shaw, *Active vibration control of a flexible beam using a buckling-type end force*, Journal of Dynamic Systems, Measurement, and Control, Vol. 128, No. 2 (2006).

[8] J. Issa, R. Mukherjee, S.W. Shaw, *Vibration suppression in structures using cable actuators*, Journal of Vibration and Acoustics, Vol. 132, No. 3 (2010).

[9] P. Thomson, G.J. Balas, P.H. Leo, *The use of shape memory alloys for passive structural damping*, Smart Materials and Structures, Vol. 4, No. 1 (1995).

[10] L.N. Virgin, *Vibration of Axially-Loaded Structures*, Cambridge University Press (2007).

[11] J.L. du Bois, N.A.J. Lieven, S. Adhikari, *A tensioned cable as an adaptive tuned vibration absorber for response suppression in rotorcraft*, *Proceedings of International Conference on Noise and Vibration Engineering*, (2012).

[12] J.C. Houbolt, G.W. Brooks, *Differential equations of motion for combined flapwise bending, chordwise bending, and torsion of twisted nonuniform rotor blades*, NACA Technical Note 3905 (1957).

[13] A.H. Nayfeh, P.F. Pai, *Linear and Nonlinear Structural Mechanics*, Wiley (2008).

[14] M. Rafiee, F. Nitzsche, M. Labrosse, *Dynamics, vibration and control of rotating composite beams and blades: A critical review*, Thin-Walled Structures, Vol. 119 (2017), pp. 795-819.

[15] V.Z. Vlasov, *Thin-walled Elastic Beams*, The Israel Program for Scientific Translations Ltd (1961).

[16] Z.P. Bazant, L. Cedolin, *Stability of Structures: Elastic, Inelastic, Fracture and Damage Theories*, World Scientific (2010).

[17] S.H.R. Eslimy-Isfahany, J.R. Banerjee, *Dynamic response of an axially loaded bending-torsion coupled beam*, Journal of Aircraft, Vol. 33, No. 3 (1996), pp. 601-607.

[18] J. Kierzenka, L.F. Shampine, *A BVP solver based on residual control and the Matlab PSE*, ACM Transactions on Mathematical Software, Vol. 27, No. 3 (2001), pp. 299-316.

[19] J.S. Bendat, A.G. Piersol, *Random Data: Analysis and Measurement Procedures*, John Wiley & Sons, Inc. (2000).

[20] B. Peeters, H. Van Der Auweraer, P. Guillaume, J. Leuridan, *The PolyMAX frequency-domain method: a new standard for modal parameter estimation?*, Shock and Vibration, Vol. 11 (2004), pp. 395-409.

[21] A. Brocklehurst, G.N. Barakos, *A review of helicopter rotor blade tip shapes*, Progress in Aerospace Sciences, Vol. 56 (2013), pp. 35-74.

[22] D.H. Hodges, E.H. Dowell, *Nonlinear equations of motion for the elastic bending and torsion of twisted nonuniform rotor blades*, NASA Technical Note D-7818 (1974).

[23] J.S. Arora, *Introduction to Optimum Design*, Academic Press (2011).

[24] D.H. Hodges, *Nonlinear Composite Beam Theory*, American Institute of Aeronautics and Astronautics (2006).

[25] C.W. Bert, M. Malik, *Differential quadrature method in computational mechanics: A review*, Applied Mechanics Reviews, Vol. 49, No. 1 (1996), pp. 1-28.